The Ciência & Engenharia - Science & Engineering Journal
ISSN: 0103-944X
Volume 11 Issue 1, 2023
pp: 138 - 153

Precise Identification and Quantitative Analysis of Right Ventricle Using Hierarchical Intensity Clustering with Markov Random Field for Cardiac Mr Images

Anjali Abhijit Yadav

Department of Electronics and Telecommunication, SPPU‘s Sinhgad College of Engineering, , Pune, Maharashtra, 411041, India
yadavanjali2k18@gmail.com

Sanjay R. Ganorkar

Department of Electronics and Telecommunication, SPPU‘s Sinhgad College of Engineering, , Pune, Maharashtra, 411041, India
srganorkar.scoe@ sinhgad.edu

Sanjeevani Shah

Department of Electronics and Telecommunication, SPPU‘s Sinhgad College of Engineering, , Pune, Maharashtra, 411041, India
skshah@gmail.com

Abstract

Precise localization and quantitative analysis of the right ventricle from cardiac magnetic resonance imaging (CMRI) images is imperative for assessing cardiopulmonary and cardiovascular mal-functionalities. Due to its poorly defined borders, precise contouring of the RV in CMRI images continues to be difficult. An approach for contouring the right ventricle based on a hierarchical intensity-based clustering method followed by Markov random field is proposed in this paper to overcome this difficulty.Because our method offers localization for each time step, it enables comprehensive right ventricle analysis during the whole cardiac-cycle. It also allows automatic prediction systems of volumetric parameters such as end systole and end diastolestages.48 human participants' cardiac MRI scans were used to validate the method. The presented scheme yielded significantly less variance than (approximately one half) compared to the reference standard of manually determined RV contours by clinical experts. This approach obtained mean Dice-Coefficient and Haussdorff-Distance of 0.92 and 5.25 mm 0.94 and 5.68 mm on the validation and tests. Further the results are evaluated using diagnosis metrics such as end diastole volume, end systole volume, and ejection fraction. Our model heading towards accurate RV localization at endocardium borders in cardiac MRI.

Keywords: Magnetic resonance imaging, Right Ventricle, Markov random Field.

The Ciência & Engenharia - Science & Engineering Journal
ISSN: 0103-944X
Volume 11 Issue 1, 2023
pp: 138 - 153

1. Introduction

As per World Health Organization research [1] cardiovascular and cerebrovascular disorders are the major causes of death and mortality globally, and they still represent a severe health risk to humans. The amount contained by the epi-cardium borders of the right ventricle (RV) must be calculated in order to evaluate a variety of cardiovascular as well as cardiopulmonary illnesses [2] [3]. A etiologies of right ventricular (RV) failure encompass 1. portal hypertension, 2. congenital heart defects, 3. cardiomyopathy, 4. myocardial infarction (MI) and 5. septic [4]. Despite clinical findings from multiple studies [5–6], the significance of RV exploration was disregarded in the recent decade. During a normal CMRI, a series short axis (SA) slices encompassing entire RV through base to apex are obtained. Precisely delineated scans are then fragmented to outline the RV borders and the end systole (ESV) and end diastole volumes (EDV) are estimated to cost the various RV clinical characteristics. Consequently, segmentation of the RV remains difficult, owing to blood-motion, the rapid heartening and obstructive imaging [7][8]. The RV seems to be more challenging to segment than the LV because of its changeable and uneven structure, as well as thin and ill-defined borders. Despite the fact that numerous automated or semi-automated techniques to LV-segmentation had implemented [9–12], the RV is nevertheless manually contoured in clinical practice. To increase the performance of RV-based diagnostics, rapid and worthwhile automated and semi-automated techniques for identification of RV must be studied.

Manual RV delineation from short-axis CMRIs' and long-axis CMRIs' are imprecise as well as time-consuming. The automated RV localization quiet difficult, owing to diverse intensity, complicated changing forms, and an ambiguous RV border [13]. RV localization automated methods are trending toward learning based strategies evolved. To emerge these approaches, adequate, big, and tagged data are required. The following benefits of the proposed strategy over previous RV precise localization:

(1) It eliminates the need of manually-arduous constructed training-sets;
(2) It makes no prior-localizations about shape distributions;
(3) It offers a successive data point gradually, an extensive input that can be very beneficial in ventricular regional wall motion analysis applications apart from identification.
(4) It is offers adaptable identification of congenital cardiopathies, when RV varies greatly in form.

2. Literature Survey

Right ventricle is the cardiac chamber responsible for exhilarating blood impoverished in oxygen to the lungs. It is located in the heart's lower right quadrant, beneath the right atrium and opposite the left ventricle. Deoxygenated blood enters the right atrium and travels via the tricuspid valve to the right ventricle, where it is pushed up through the pulmonary valve and into lungs through the pulmonary artery. The right ventricle is in charge of moving blood from the right atrium to the pulmonary trunk, ultimately to the lungs through the pulmonary

The Ciência & Engenharia - Science & Engineering Journal
ISSN: 0103-944X
Volume 11 Issue 1, 2023
pp: 138 - 153

arteries. Extraction requires precise identification of the right and left ventricles (LV). The segmentation of a complicated anatomy of a RV chamber in CMRI is the most difficult. The trabeculations in the RV vary in signal strength and form from base to apex, as in a crescent shape myocardiums complicated, depending on strong augmentations and imaging procedure. N. Das et al. [14] conduct a survey of RV segmentation techniques. Li, L., et al.,[15] offer an automated RV segmentation framework in which input from long-axis (LA) views is used to help with short-axis (SA) view segmentation through information transition.

The information transfer tries to reduce the unclear zones around the SA perspectives. Arega, T., et al. [16] describe a completely autonomous deep learning system that utilises several data augmentation strategies to address the issue. A. Khalil et al. [17] create a model that uses image synthesis as well as multi-fusion segmentation to segment all tri-cardiac components. Ammari, A et al. [18] developed a customizable method for extracting and annotating informative slices, beginning with complete CMRI sequences. H. El-Rewaidy et al.[19] present a work for modelling the RV surface utilizing various 2Dcontours, including information from various trans-sectional scans into the single set. X. Huang et al. [20] introduced RegUNet, a new regionlevel U-Net contouring approach for ventricular localization. RegUNet enhances ventricular segmentation-fidelity by first collecting the ventricle’s area of interest and afterwards segmenting the ventricular using the collected RoI features, reducing the complexity of the contouring module by retaining the cardiac's characteristics. D. Liu et al. [21] provide a unique paradigm for segmenting the ventricles in both short-imaging n longitudinal axis imaging.

The approach segments the two views individually at first, and then refines their segmentations by combining complementing data from the other perspectives. X. Shi et al. [22] describe a new level set framework for segmenting cardiac left ventricle (LV) and right ventricle (RV) from MRI using anatomical heart features. M. Ng et al. [23] conducted a thorough investigation of Bayesian and NonBayesian approaches for assessing ambiguity in segmentation neural networks. J. Chen et al. [24] offer a class dependent feature deracination strategy in which task-learning module is created. S. Dong et al.,[25] offer a new framework for trans-modality cardiac image localization called Partial Un-balanced feature transport that incorporates continuous normalizing flows into extended variational Auto Encoders to estimate the probabilistic posterior and reduce inference bias.

A. Ammari et al. [26] presented a pipelined architecture that includes customized dataset labelling as well as augmentation to enable for early learning. Second, a U-Net-based design is optimized for accuracy. Ultimately, a two-level uncertainty assessment approach is agreed upon to allow for the selection of comparable unlabeled data. J. kesson et al. [27] set out to create a medical pipeline for deep learning-based RV differentiations and test its capacity to minimize manual delineation time. Z. Guo et al. [28] suggested LMIC model-based technique for segmenting the RV. Due to cardiac motion and blood flow, the LMIC method incorporates the local intensity clustering features and motion intensity information [34]. J. Ringenberg et al. [29] provide a completely automated approach for segmenting the RV using

The Ciência & Engenharia - Science & Engineering Journal
ISSN: 0103-944X
Volume 11 Issue 1, 2023
pp: 138 - 153

short-axis CMRI. To drive the segmentation, an unique window-constrained accumulator thresholding approach, binary difference of Gaussian (DoG) filters, optimum thresholding, and morphology are used. M. Zuluaga et al. [30, 34] provide a completely automated approach for segmenting the RV in cardiac MRI). A coarse-to-fine segmentation technique is used with a multi-atlas diffusion segmentation framework in the method [31, 32, 33].

3. Methodology

After providing a short overview of fuzzy clustering and level-set approaches in Sections A and B, respectively, Section C describes the suggested approach.

FCM Clustering:

By dividing the image into a set of c distinct regions $\{\mathcal{R}_i\}$ that are maximally linked and each $\mathcal{R}_i$ is coherent according to certain criteria; image segmentation seeks to create meaningful groups of pixels with similar intensity values. Locating if a particular pixel belongs to an area is often challenging. Fuzzy set ideas are used in the segmentation process to handle this kind of issue. When it comes to fuzzy clustering techniques for medical image segmentation, FCM (Fuzzy C-mean) is among the most popular options.

FCM partitions $\{x_k\}_{k=1}^{N}$ clusters by minimising an objective function such as:

$$J = \sum_{i=1}^{c}\sum_{k=1}^{N} u_{ik}^{m}\|x_k - v_i\|^2 \qquad [1]$$

$$x_k = \text{Gray Value associated with } k^{\text{th}} \text{ pixel}$$

$$v_i = i^{\text{th}}\text{Cluster Center}$$

$$u_{ik} = \text{Fuzzy menmbership Value of pixel } k$$

$$m = \text{Fuzziness Exponent with valuelarger than 1}$$

Output of FCM clustering contain three cluster of black, gray and white pixels. RV are is not fully segment in this step. For fine segmentation of RV region those clusters are forwarded to Level set function.

Level Set Function

The foundation of active contour techniques is the iterative motion of the contour while adhering to certain limitations in relation to the original image. If the target object for detection is already present in the image, the contour will begin over it and move toward the item's inner normal. Osher and Sethian's 1988 LMS employs a 2DLipschitz function as level-set function, using the notation $\varphi(x, y)$ for the x and y coordinates, respectively.

The Ciência & Engenharia - Science & Engineering Journal
ISSN: 0103-944X
Volume 11 Issue 1, 2023
pp: 138 - 153

Contour $\mathcal{C} = \left\{\frac{(x,y)}{\varphi(x,y)} = 0\right\}$ which develops according to a time-dependent curve with zero levels at time t as $\varphi(x, y)$.

The equation for the levelset function is represented by the following partial differential equation:

$$\frac{\partial \varphi}{\partial t} = |\nabla \varphi| \mathcal{F}\,, \varphi(0, x, y) = \varphi_0(x, y) \qquad [2]$$

Here, (0,x,y) represents the starting contour and F stands for both external and internal forces.

Precise Identification of RV:

Initially, the suggested technique would segment the ROI using a level set method and fuzzy clustering. In the suggested method, the level set function is initialized to an initial value using fuzzy clustering. The FCM produces artefacts like the blobs and the outliers shown in the image. With the use of Gaussian Filtering, these by products may be disentangled. Afterwards, the level-set function is first established using the output of the fuzzy clustering procedure.

$$\mathcal{M}_{i,j} = \text{Membership Function}$$

$$\mathcal{Z}_{i,j} = \text{ROI extracted fromImage}$$

ROI is extracted as,

$$\mathcal{Z}_{i,j} = \begin{cases} 1, & u_{ij} > b_0 \\ 0, & otherwise \end{cases}$$

$$b_0 \in (0,1)\ is \text{ adjustable threshold}$$

The level-set function is set up initially as:

$$\varphi_0(x, y) = 2\varepsilon\left(2\mathcal{Z}_{i,j} - 1\right) \qquad [3]$$

$$\varepsilon = \text{ constant meant for regularizing the Dirac function}$$

In traditional level set approaches, the growth of the level-set function is controlled by manually inputting a number of regulating parameters with values that change according to the desired application. The suggested technique utilizes the outputs of fuzzy segmentation to perform an adaptive evaluation of all the necessary controlling parameters. Fuzzy clustering's area and the length of the related contour are measured using the Heaviside and Dirac functions.

$$\mathcal{C}_{\text{Area}}(\varphi \geq 0) = \int_{-\Omega}^{\Omega} \mathcal{H}\left(\varphi(x, y)\right) dx\, dy \qquad [4]$$

$$\mathcal{C}_{\text{Length}}(\varphi = 0) = \int_{-\Omega}^{\Omega} \delta_0\left(\varphi(x, y)\right) |\nabla \varphi(x, y)| dx\, dy \qquad [5]$$

The Ciência & Engenharia - Science & Engineering Journal
ISSN: 0103-944X
Volume 11 Issue 1, 2023
pp: 138 - 153

Here, the Heaviside function may be described as:

$$\mathcal{H}(\varphi) = \begin{cases} 1, & if\ \varphi \geq 0 \\ 0, & if\ \varphi < 0 \end{cases} \quad [6]$$

along with the Dirac function as

$$\delta_0(\varphi) = \frac{d}{d\varphi}\,\mathcal{H}(\varphi) \quad [7]$$

Caused by the balloon's internal pressure The extraction zone is drawn in by the level-set function, which is generated by the parameter m. Depending on the sign of m, the balloon force contracts or expands the level-set function, eliminating the need to initialise the function in close proximity to the limits of the needed object. The pressure is represented by the magnitude of m, which is shown to be big enough to squeeze through artificial boundaries. Thus, in the suggested approach, the value of m is calculated based on the output of the fuzzy segmentation as:

$$\mathcal{v} = 0.5 - \mathcal{u}_{i,j} \quad [8]$$

$\mathcal{u}_{i,j}$ = membership function associated with fuzzy segmentation for every pixel

Markov Random Field (MRF) is a robust stochastic modelling method that may efficiently depict local interactions between neighbouring pixel characteristics. Further, it can represent the spatial relationship between neighbouring pixels in terms of probability distributions in a Bayesian setting. Maximum a posteriori (MAP) labelling space segmentation is performed based on the images provided. Energy maximisation problems are at the heart of the MRF MAP specifications. In addition to the combinatorial nature of the maximisation problem, the non convexity of the energy function and the presence of several local minima in the image's solution space make this a particularly challenging problem to solve. Hidden Markov Random Field (HMRF) is a revolutionary approach that was developed as an offshoot of the original Hidden Markov Model, which is a Markov chain-based algorithm. The right states of HMRF are not directly observed but rather approximated through a circuitous observation field, making it a graphical probability prototype.

In a HMRF model, there is an observable random field,

$$a = (a_1, \ldots, a_N)$$

$$a_i = \text{Feature Value of Pixel}$$

That seeks to deduce a secret random field

$$\text{Hidden Random Field} = (\mathcal{b}_1, \ldots, \mathcal{b}_N)$$

$$\mathcal{b}_i \in \mathcal{K}$$

$$\mathcal{K} = \text{set of all possible labels.}$$

The Ciência & Engenharia - Science & Engineering Journal
ISSN: 0103-944X
Volume 11 Issue 1, 2023
pp: 138 - 153

$$\mathcal{b}_i = \text{configuration of labels}$$

The label field a_i Regarding its surrounding system, it would be an MRF if the following Markovian characteristic held.

$$\rho(a|\mathcal{b}) = \prod_{i\in\mathcal{S}} \rho(a_i|\mathcal{b}_i) \qquad [9]$$

$\mathcal{S}$ *Spot related to another one another with neighbourhood System*

$$\mathcal{N} = \{\mathcal{N}_i, i \in \mathcal{S}\}$$

$$\mathcal{N}_i = \text{ pots adjacent to pixel } i$$

$$\mathcal{b}_{\mathcal{N}i} = \text{Neighbourhood Configuration}$$

Equation 9 of the Modified Rayleigh Felt (MRF) expresses the conditional independences between variables as

$$\rho(a|\mathcal{b}) = \rho(a|\mathcal{b})\rho(x) = \rho(\mathcal{b}) \prod_{i\in\mathcal{S}} \rho(a_i|\mathcal{b}_i) \qquad [10]$$

$$\rho(a_i, \mathcal{b}_i|\mathcal{b}_{\mathcal{N}i}) = \rho(a_i|\mathcal{b}_i)\rho(\mathcal{b}_i|\mathcal{b}_{\mathcal{N}i}) \qquad [11]$$

Assume that a is drawn from a probability function, $f(a; \mathcal{k}, \theta)$, for $\mathcal{k} \in \mathcal{K}$ and the marginal distribution of a_i is obtained as:

$$\rho(a_i|\mathcal{b}_{\mathcal{N}i}, \theta) = \sum_{\mathcal{k}\in\mathcal{K}} \rho(a_i, \mathcal{k}|\mathcal{b}_{\mathcal{N}i}, \theta) = f(a_i, \theta_{\mathcal{k}})\, \rho(\mathcal{k}|\mathcal{b}_{\mathcal{N}i}) \qquad [12]$$

The EM Algorithm for HMRF Estimation:

$$\widehat{\mathcal{b}} = \arg\max_{\mathcal{b}} \{\rho(a|\mathcal{b}, \Theta)\rho(\mathcal{b})\} \qquad [13]$$

An MRF can equivalently be characterized by a Gibbs distribution:

$$\rho(\mathcal{b}) = z^{-1} exp\left(-\mathcal{V}_{(\mathcal{b})}\right) \qquad [14]$$

$$z: \text{normalization constant}$$

$$\mathcal{V}_{(\mathcal{b})} = \text{potential function}$$

The prior probability $\rho(\mathcal{b})$ is a Gibbs distribution in Equation [z6], its joint probability is written as

$$\rho(a|\mathcal{b}, \Theta) = \prod_i \rho(a_i|\mathcal{b}, \Theta) = \prod_i \rho(a_i|\mathcal{b}_i, \theta_{\mathcal{b}i}) \qquad [z7]$$

$$\rho(a_i|\mathcal{b}_i, \theta_{\mathcal{b}i}): \text{Gaussian distribution with parameters}$$

$$\theta_{\mathcal{b}i} = (\mu_{\mathcal{b}i}, \Sigma_{\mathcal{b}i})$$

The Ciência & Engenharia - Science & Engineering Journal
ISSN: 0103-944X
Volume 11 Issue 1, 2023
pp: 138 - 153

The HMRF-EM algorithm is can be written as,

Step 1: Launch parameterization

Step 2: Determine the probability distribution. $\rho(a_i|\mathcal{b}_i, \theta_{\mathcal{b}i})$

Step 3: Using $\Theta^{(t)}$ to calculate labels by MAP estimation:

$$\mathcal{b}^{(t)} = \arg\max_{\mathcal{b}\in\mathcal{B}}\{\rho(a|\mathcal{b}, \Theta^{(t)})\rho(\mathcal{b})\}$$

$$= \arg\min_{\mathcal{b}\in\mathcal{B}}\{\mathcal{V}(a|\mathcal{b}, \Theta^{(t)}) + \mathcal{V}(\mathcal{b})\} \quad [z7]$$

Step 4: Calculating the posterior distribution $\mathcal{k} \in \mathcal{K}$ and pixels a_i,

$$\rho^{(t)}(\mathcal{k}|a_i) = \frac{\mathcal{N}(a_i, \theta_i)\rho\left(\mathcal{k}\middle|\mathcal{b}_{\mathcal{N}_i}^{(t)}\right)}{\rho^{(t)}\mathcal{b}_i}$$

$$\mathcal{N}(a_i, \theta_i) = \text{Gaussian Distribution of } a_i \text{ with}$$

$$\theta_{\mathcal{k}} = (\mu_{\mathcal{k}}, \Sigma_{\mathcal{k}})$$

$$\rho\left(\mathcal{k}\middle|\mathcal{b}_{\mathcal{N}_i}^{(t)}\right) = \frac{1}{z}\exp\left(-\sum_{j\in\mathcal{N}_i}\mathcal{V}_c\left(\mathcal{k}, \mathcal{b}_j^{(t)}\right)\right)$$

Step 5: To modify the parameters of a Gaussian distribution, $\rho\left(\mathcal{k}|\mathcal{b}_{\mathcal{N}_i}^{(t)}\right)$.

Before using HMRF-EM, the HMRF technique for image segmentation generates an initial segmentation based on the gray-level intensities of pixels, utilising FCM clustering. Its relevance is shown by the fact that less iteration are required to produce final labels using this method than using the MRF-MAP method.

In the suggested technique, the initial segmentation of images is calculated based on the energy functions established for the combination of Clustering based Levelset and MRF. Most often, the Potts model presents the local prior energy function, also known as the potential function, as,

$$\mathcal{E} = -\sum_{j\in\mathcal{N}_i}\mathcal{V}_c\left(\mathcal{k}, \mathcal{b}_j^{(t)}\right)$$

$$\mathcal{V}_c = \text{Kronecker delta which equals 1 for } \mathcal{k} = \mathcal{b}_j^{(t)} \text{ and being 0 otherwise.}$$

In addition, the posterior energy function requires modelling the image's probability density function.

The Ciência & Engenharia - Science & Engineering Journal
ISSN: 0103-944X
Volume 11 Issue 1, 2023
pp: 138 - 153

Experiments & Results

The MRF provides the outcome of image segmentation by saving energy. The approach of energy minimization is compatible with the strategy stated above. Figure 1 shows the precise identification of the right ventricles from an MRI image. The right-side image depicts predictions, whereas the left-most image depicts expert's contoured images utilized for performance computation. Our model tackles imaging noise interference and intensity-unequality by enhancing image intensity homogeneity in the areas of interest; however, it is unable to differentiate between RV and subcutaneous tissue on initial images.

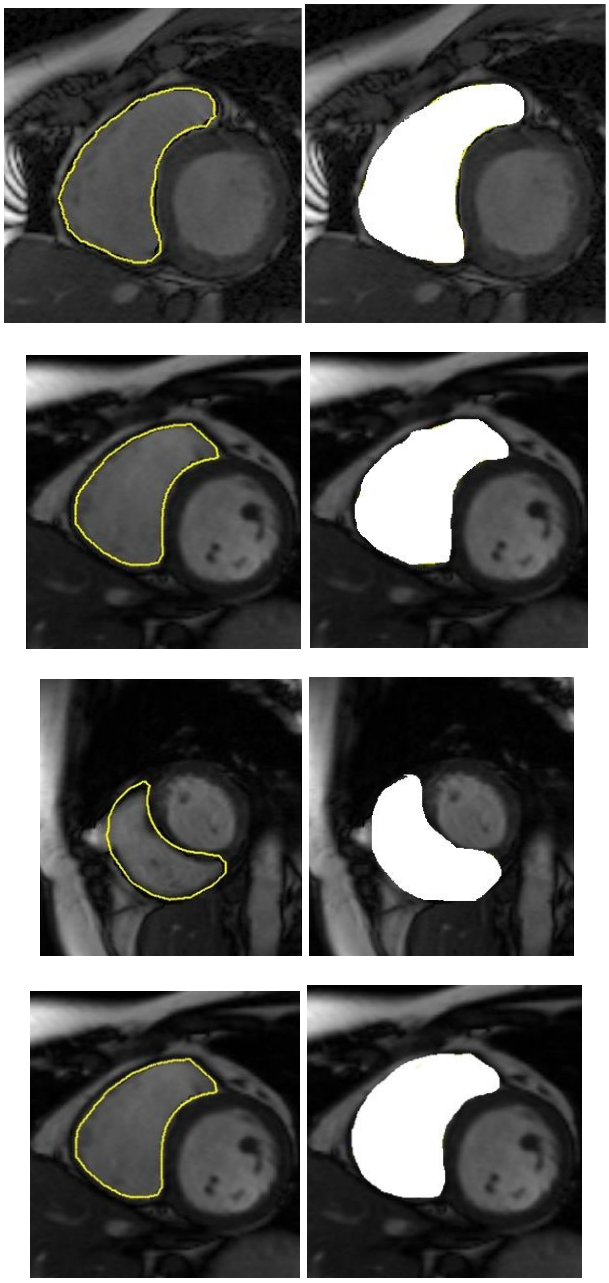

Fig 1: Segmentation results obtained with proposed method. (Left: Predicted ROI, Right: Ground Truth)

The Ciência & Engenharia - Science & Engineering Journal
ISSN: 0103-944X
Volume 11 Issue 1, 2023
pp: 138 - 153

To quantitative-assess the effectiveness of the suggested technique, the precise identification of RV was compared to the using two parameters.

Dice-Coefficient:

Dice-Coefficient (DM) computes the ratio of overlap as the total of human and automated segmentations to determine the similarity of two areas. DM is administered via

$$DM = \frac{2 \ * \ \text{Area of Overlap}}{\text{total pixels combined}}$$

DM ranges from 0 to 1. With 0 indicating complete mismatch and 1 indicating perfect fit.

Haussdorff-Distance:

To quantify the distance between two contours, the Haussdorff-Distance (HD) approximates the value of the largest disagreement from point to curve between the actualto automated contours.

$$HD = \min_{a \in A}\left(\min_{b \in B}(d\{a, b\})\right)$$

Following table represent performance analysis of testing data, where proposed method archives better DM and HD than rest of the methods.

Table:1 Comparison of DM and HD for Testing dataset

Method	**DM**	**HD**
Proposed	0.92	5.25
Z. Guo et al.,[28]	0.91	6.73
Ringenberg et al [29]	0.83	9.05
Zuluaga et al [30]	0.78	10.51

Following table represent the performance analysis of validation data, where proposed method archives better DM and HD than rest of the methods.

Table: 2 Comparison of DM and HD for Validation dataset

Method	**DM**	**HD**
Proposed	0.94	5.68
Z. Guo et al.,[28]	0.93	5.71
Ringenberg et al [29]	0.83	8.73
Zuluaga et al [30]	0.73	12.5

The Ciência & Engenharia - Science & Engineering Journal
ISSN: 0103-944X
Volume 11 Issue 1, 2023
pp: 138 - 153

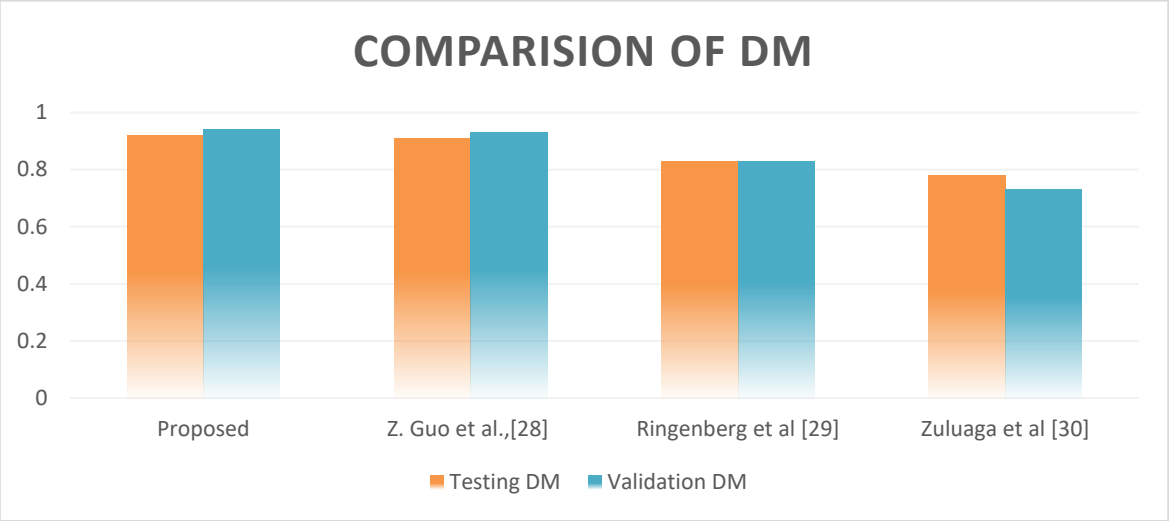

Fig 2: Testing and Validation dataset DM values

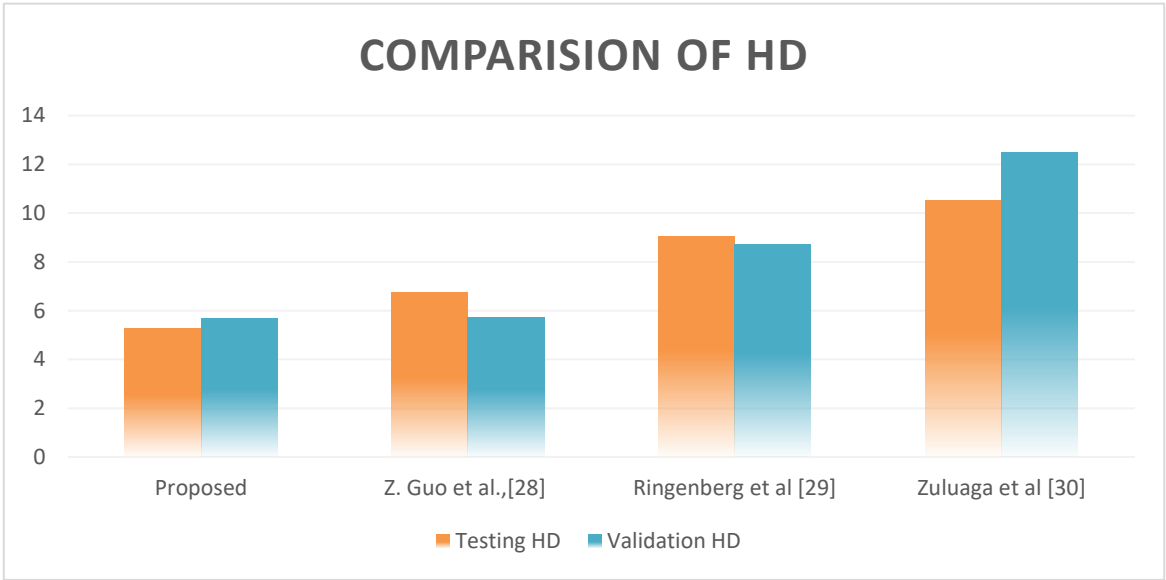

Fig 3: Testing and Validation dataset HD values

Proposed method HD and DM graphs are shown above.

The further accomplishment of proposed method is estimated for systole volume, diastole volume, ejection fraction (EF) and Bland-Altman plot. Endocardial volumes are computed as successive defalcation of extracted RV areas multiplied with the space between slices value. It is the absolute difference between Slice places in the DICOM field in two neighboring images. The 8.4mm SpaceBetweenSlices is provided in dataset for all patients. ESV volumes are calculated as the total of all right ventricle regions of systolic frames multiplied by the value of the space between slices. It is used in cardiac function idiosyncrasy and calculation of ejection-fraction and stroke-volume. EDV volumes calculated as the summation of all RV regions of diastolic frames multiplied by the value of the space between slices. It is used to estimate preload of heart, EF and stroke volume. Ejection fraction is calculated using

The Ciência & Engenharia - Science & Engineering Journal
ISSN: 0103-944X
Volume 11 Issue 1, 2023
pp: 138 - 153

difference of EDV and ESV divided by EDV. It is used to determine how well the heart is pumping blood [31].

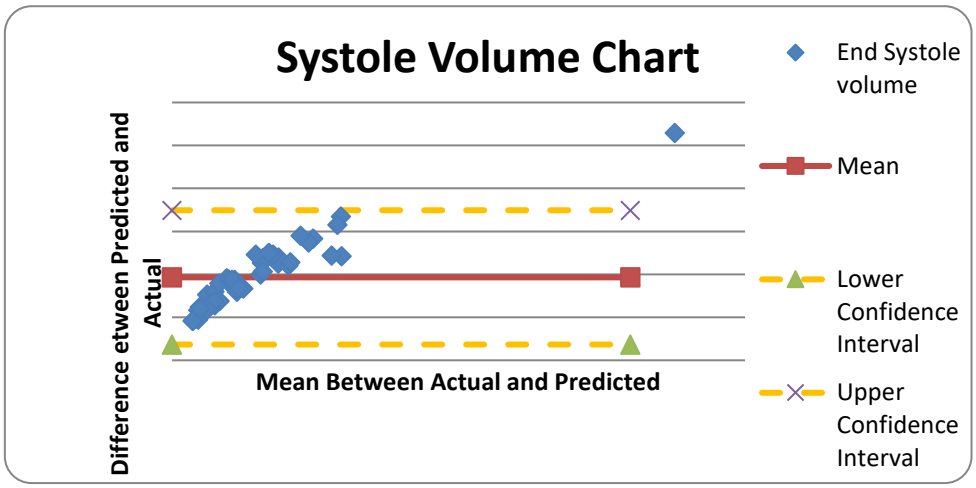

Fig 4: Bland-Altman Plot for systolic volume

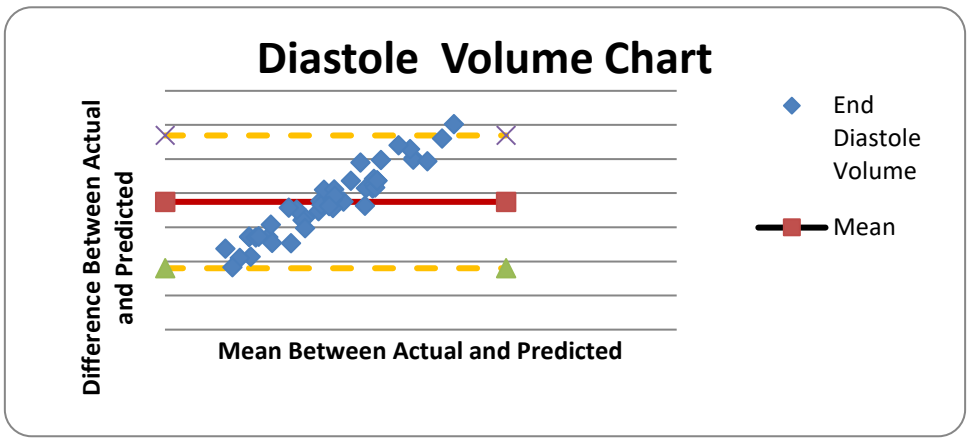

Fig 6: Bland-Altman Plot for Diastolic Volume

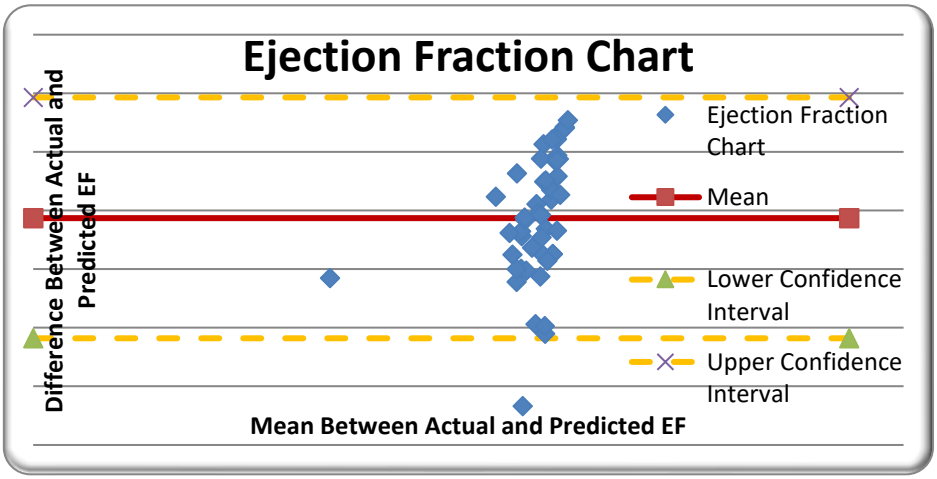

Fig 7: Bland-Altman Plot for Ejection Fraction

The Ciência & Engenharia - Science & Engineering Journal
ISSN: 0103-944X
Volume 11 Issue 1, 2023
pp: 138 - 153

Bland-Altman plotting is an immaculate way to determine two techniques. Fig. 5, 6 and 7 views Bland-Altman scheme for volumetric measurements and Ejection Fraction parameter for right ventricle. The results show that predicted results by proposed method are within acceptable convergence level.

Conclusion

Right ventricular localization is critical for cardiac diagnosis. The Right Ventricle (RV) is preeminently substantial, crucial prognostic factor for a variety of diseases. However, it is hampered by several anatomical and imaging difficulties. Our implementation is an approach for precise identification and localization of the RV based on a hierarchical intensity clustering technique followed by a Markov random field. The results are in acceptable level. On the validation and test sets, the suggested technique obtained an average total Dice score and Haussdorff distance of 0.92 and 5.25 mm, 0.94 and 5.68 mm. Then further the results are verified with actual and predicted parameters end systole volume, end diastole volume and EF. These findings show that the suggested approach has the capacity to accurately segment RVs in cardiac MRI. In regards of segmentation accuracy and method durability, our technique is equivalent to the state-of-the-art technique, but it does not need training or human segmentation of the training data.

References

[1] World Health Organization. Cardiovascular diseases (CVDs)[EB/OL] Fact Sheet NO. 317, [2017-05]. http://www.who.int/mediacentre/factsheets/fs317/en

[2] D. Groote et.al. (1998), Right ventricular ejection fraction is an independent predictor of survival in

patients with moderate heart failure. J Am Coll Cardiol. Oct;32(4):948-54. PMID: 9768716. https://doi.org/10.1016/s0735-1097(98)00337-4.

[3] Matthews J. et.al.. (2008), Right-sided heart failure: diagnosis and treatment strategies. Curr Treat Options Cardiovasc Med., Aug;10(4):329-41. doi: 10.1007/s11936-008-0053-6. PMID: 18647588.

[4] D. Groote et.al., (1998), Right ventricular ejection fraction is an independent predictor of survival in patients with moderate heart failure. J Am CollCardiol., Oct;32(4):948-54. https://doi.org/10.1016/s0735-1097(98)00337-4. PMID: 9768716.

[5] Andersen HR, Falk E, Nielsen D. (1987), Right ventricular infarction: frequency, size and topography in coronary heart disease: a prospective study comprising 107 consecutive autopsies from a coronary care unit. J Am CollCardiol., Dec;10(6):1223-32. https://doi.org/10.1016/s0735-1097(87)80122-5. PMID: 3680789.

[6] Palevsky H.et.al. (1990), Chronic Cor Pulmonale: Etiology and Management. JAMA. 1990;263(17):2347–2353. https://doi.org/10.1001/jama.1990.03440170069039

[7] Haddad F, et.al., (2008), Right ventricular function in cardiovascular disease, part I: Anatomy, physiology, aging, and functional assessment of the right ventricle.

Circulation., Mar 18;117(11):1436-48. https://doi.org/10.1161/CIRCULATIONAHA.107.653576. PMID: 18347220.

[8] Ryan J.et.al.,(2014),The right ventricle in pulmonary arterial hypertension: disorders of metabolism, angiogenesis and adrenergic signaling in right ventricular failure. Circ Res., Jun 20;115(1):176-88. doi: 10.1161/CIRCRESAHA.113.301129. PMID: 24951766; PMCID: PMC4112290.

[9] Wang, Li et.al. ((2015), Automatic Left Ventricle Segmentation in Cardiac MRI via Level Set and Fuzzy C-Means, https://doi.org/10.1109/RAECS.2015.7453332.

[10] Santiago C, et.al. (2015), Segmentation of the left ventricle in cardiac MRI using a probabilistic data association active shape model. AnnuInt Conf IEEE Eng Med Biol Soc.; 2015:7304-7. https://doi.org/10.1109/EMBC.2015.7320078. PMID: 26737978.

[11] Wang, Li et.al. (2015), Automatic Left Ventricle Segmentation in Cardiac MRI via Level Set and Fuzzy C-Means, https://doi.org/10.1109/RAECS.2015.7453332.

[12] A. Bhan, et.al., (2015), Fast fully automatic multiframe segmentation of left ventricle in cardiac MRI images using local adaptive k-means clustering and connected component labeling, 2nd International Conference on Signal Processing and Integrated Networks (SPIN), Noida, India, pp. 114-119, https://doi.org/10.1109/SPIN.2015.7095354.

[13] J. Chen, et.al., (2018), Correlated Regression Feature Learning for Automated Right Ventricle Segmentation, IEEE Journal of Translational Engineering in Health and Medicine, vol. 6, pp. 1-10, Art no. 1800610, https://doi.org/10.1109/JTEHM.2018.2804947.

[14] N. Das et.al. (2022), A review on right ventricle cardiac MRI segmentation, Computer Methods in Biomechanics and Biomedical Engineering: Imaging & Visualization, DOI: 10.1080/21681163.2022.2125697

[15] Li, L., et.al., (2022), Right Ventricular Segmentation from Short- and Long-Axis MRIs via Information Transition. In: , et al. Statistical Atlases and Computational Models of the Heart. Multi-Disease, Multi-View, and Multi-Center Right Ventricular Segmentation in Cardiac MRI Challenge. STACOM 2021. Lecture Notes in Computer Science, vol 13131. Springer, Cham, https://doi.org/10.1007/978-3-030-93722-5_28

[16] Arega, T.et.al. (2022), Using MRI-specific Data Augmentation to Enhance the Segmentation of Right Ventricle in Multi-disease, Multi-center and Multi-view Cardiac MRI. In: , et al. Statistical Atlases and Computational Models of the Heart. Multi-Disease, Multi-View, and Multi-Center Right Ventricular Segmentation in Cardiac MRI Challenge. STACOM 2021. Lecture Notes in Computer Science(), vol 13131. Springer, Cham, https://doi.org/10.1007/978-3-030-93722-5_27

[17] A. Khalil, et.al., (2022), Late Fusion U-Net with GAN-Based Augmentation for Generalizable Cardiac MRI Segmentation. In: , et al. Statistical Atlases and Computational Models of the Heart. Multi-Disease, Multi-View, and Multi-Center Right Ventricular Segmentation in Cardiac MRI Challenge. STACOM 2021. Lecture Notes in Computer Science, vol 13131. Springer, Cham.. https://doi.org/10.1007/978-3-030-93722-5_39

[18] Ammari, A., et al.(2022), Clinical-Guided Strategy Towards a Spatio-Temporal Cardiac MRI Right Ventricular Short-Axis (ST-CMRI-RVSA) Labeled Dataset. SN COMPUT. SCI. 3, 287 (2022). https://doi.org/10.1007/s42979-022-01144-7

[19] H. El-Rewaidyet.al.,(2022), Multiple two-dimensional active shape model framework for right ventricular segmentation, Magnetic Resonance Imaging, Volume 85, Pages 177-185, ISSN 0730-725X, https://doi.org/10.1016/j.mri.2021.10.029.

[20] X. Huang, et.al.,(2022), Left and Right Ventricular Segmentation Based on 3D Region-Aware U-Net," 2022 IEEE 35th International Symposium on Computer-Based Medical Systems (CBMS), Shenzen, China, pp. 137-142, https://doi.org/10.1109/CBMS55023.2022.00031.

[21] Liu, D., et.al., (2022), Refined Deep Layer Aggregation for Multi-Disease, Multi-View & Multi-Center Cardiac MR Segmentation. In: , et al. Statistical Atlases and Computational Models of the Heart. Multi-Disease, Multi-View, and Multi-Center Right Ventricular Segmentation in Cardiac MRI Challenge. STACOM 2021. Lecture Notes in Computer Science, vol 13131. Springer, Cham., https://doi.org/10.1007/978-3-030-93722-5_34

[22] X. Shi et.al.,(2022), Anatomical knowledge based level set segmentation of cardiac ventricles from MRI, Magnetic Resonance Imaging, Volume 86, Pages 135-148, ISSN 0730-725X, https://doi.org/10.1016/j.mri.2021.10.005.

[23] M. Ng et al., (2022), Estimating Uncertainty in Neural Networks for Cardiac MRI Segmentation: A Benchmark Study," in IEEE Transactions on Biomedical Engineering, https://doi.org/10.1109/TBME.2022.3232730.

[24] J. Chen, J.et.al.(2022), Semi-supervised Unpaired Medical Image Segmentation Through Task-affinity Consistency, in IEEE Transactions on Medical Imaging, 2022, https://doi.org/10.1109/TMI.2022.3213372.

[25] S. Dong et al.,(2023), Partial Unbalanced Feature Transport for Cross-Modality Cardiac Image Segmentation, in IEEE Transactions on Medical Imaging, https://doi.org/10.1109/TMI.2023.3238067.

[26] A. Ammari, et.al.,(2023), Deep-active-learning approach towards accurate right ventricular segmentation using a two-level uncertainty estimation, Computerized Medical Imaging and Graphics, Volume 104, 102168, ISSN 0895-6111, https://doi.org/10.1016/j.compmedimag.2022.102168.

[27] Åkesson, J., et al., (2023), Deep learning can yield clinically useful right ventricular segmentations faster than fully manual analysis. Sci Rep 13, 1216. https://doi.org/10.1038/s41598-023-28348-y

[28] Z. Guo et al.,(2019), Local Motion Intensity Clustering (LMIC) Model for Segmentation of Right Ventricle in Cardiac MRI Images, in IEEE Journal of Biomedical and Health Informatics, vol. 23, no. 2, pp. 723-730, March, https://doi.org/10.1109/JBHI.2018.2821709.

[29] J. Ringenberg, et.al.(2014), Fast, accurate, and fully automatic segmentation of the right ventricle in short-axis cardiac MRI, Computerized Medical Imaging and Graphics,

Volume 38, Issue 3,Pages 190-201, ISSN 0895-6111, https://doi.org/10.1016/j.compmedimag.2013.12.011.

[30] M.. Zuluaga, et.al., (2012), Automatic right ventricle segmentation using multi-label fusion in cardiac MRI," in Medical Image Computing and Computer-Assisted Intervention, Workshop on RV Segmentation Challenge in Cardiac MRI, https://doi.org/10.48550/arXiv.2004.02317

[31] JinmingDuan, Ghalib Bello and et. al, (2018), Automatic 3D bi-ventricular segmentation of cardiac images by a shape-refined multi-task deep learning approach, 0278-0062,IEEE Transactions on Medical Imaging..

[32] C. Petitjean, M. A. Zuluaga, W. Bai, J.-N.Dacher, D. Grosgeorge,J. Caudron, S. Ruan, I. B. Ayed, M. J. Cardoso, H.-C. Chenet al.,(2015), Right ventricle segmentation from cardiac MRI: a collation study, Medical image analysis, vol. 19, no. 1, pp. 187–202. https://doi.org/10.1016/j.media.2014.10.004

[33] Liangijia Zhu, Yi Gao, Vikram Appia, Anthony Yezz,(2013), Automatic Delineation of Myocardial Wall From CT images Via Shape Segmentation and Variational Region growing, IEEE Transactionon Biomedical Engg., VOL. 60,No.10, pp. 2887-2895, Oct. https://doi.org/10.1109/TBME.2013.2266118

[34] Steffen E. Petersen, Nay Aung and et., (2017), Reference ranges for cardiac structure and function using cardiovascular magnetic resonance (CMR) in Caucasians from the UK Biobank population cohort, Journal of Cardiovascular Magnetic Resonance 19:18, DOI 10.1186/s12968-017-0327-9. https://doi.org/10.1186/s12968-017-0327-9

Authors Profile

Please put here scanned author's photo 3 x 4 cm.	**Full Author's Name**, Short CV of author (10-20 lines), including: education, current position and areas of scientific interests, scanned photo.
	**Anjali Abhijit Yadav, Persuing Ph.D. from** Sinhgad college of engineering, Pune, Maharashtra.
	**Sanjay Ramchandra Ganorkar,** Professor at Sinhgad college of engineering, Pune, Maharashtra.